Robust Realization/Identification Of Damped Structures

Michael J. Roemer† *and* **D. Joseph Mook***

Department of Mechanical and Aerospace Engineering
State University of New York at Buffalo
Buffalo, New York 14260

Abstract

Often, physical structures are sufficiently complicated to preclude constructing an accurate mathematical model of the system dynamics from simple analysis using the laws of physics. Consequently, determination of an accurate model requires utilization of (generally noisy) output measurements from dynamic tests. In this paper, we present a robust method for constructing accurate structural dynamic models from discrete time-domain measurements. The method processes the measurements in order to determine the number of modes present, the damping and frequency of each mode, and the mode shape. The structure may be highly damped. Although the mode shape identification is more sensitive to measurement noise than the order, frequency, and damping identification, the method is considerably less sensitive to noise than other leading methods. Accurate detection of the modal parameters and mode shapes is demonstrated for normal and complex mode structures whose damping ratios exceed 15 percent.

† Graduate Research Assistant
* Assistant Professor

Introduction

The enduring problem of accurately identifying the mode shapes of structures and/or systems using (noisy) output measurements is of significant importance in several aspects of mechanical and aerospace engineering. For example, the structural community has expended considerable effort attempting to correctly identify modal properties of flexible structures (Hendricks[1]; Ibrahim and Mikulcik[2]; Rajaram and Junkins[3]; Chen[4]). However, mode shape identification methods are very sensitive to measurement noise, and lose accuracy in high measurement noise circumstances. Addressing this problem, the paper develops an algorithm that aids in accurately identifying mode shapes of a structure from output measurements. The algorithm combines a recently developed identification/realization technique with a method of model error reduction to successfully identify mode shapes even with high noise levels in the measurements. Note; modal properties refers to: (1) natural frequencies and damping ratios, and (2) mode shapes.

Recently, the Eigensystem Realization Algorithm (ERA) was developed by Juang and Pappa[5]; Pappa and Juang[6]. The algorithm was developed for the realization and identification of minimum order structural dynamic models. The ERA technique is based on the singular value decomposition of a generalized Hankel matrix composed of discrete, time-domain measurements. In theory, the order of the realized model is determined from the number of nonzero singular values computed from the Hankel matrix decomposition. However, due to the "real world" presence of noise in the output measurements, the decomposition produces nonzero singular values which should (in theory) be zeros. Consequently, the user must choose a "cutoff" magnitude of singular values, below which the singular values are assumed to be due to noise and not due to extra order in the model. In a paper extending their original work, Juang and Pappa[7]conducted an investigation studying the effects of singular value truncation. Their results show that the choice of singular value cutoff affects the number of modes retained in the realization and the accuracy of the modal properties identified. Choosing a low cutoff produces a model which includes more modes than the true number, and results in reduced accuracy of the identified modal properties. Conversely, choosing a high cutoff results in a lower order model (some real modes are truncated), but produces better accuracy in identifying the modal properties of the retained modes. Therefore, the difficult choice of an appropriate cutoff magnitude when a high degree of noise is present is of great importance for accurate mode shape identification.

The ERA technique is capable of accurately identifying modal properties for cases involving perfect or low-noise measurements. The procedure of singular value decomposition, as opposed to transfer function analysis, has the benefit of good numerical stability (Klema and Laub[8]), and the ERA is simple to implement and accurate. However, difficulties may arise when high noise levels are present in the output measurements.

Reducing the noise sensitivity of the Eigensystem Realization Algorithm was first investigated by Mook and Lew[9], whose results were based on the simulation of a structure with a three mode truth. Given a highly noisy measurement set (20% deviation from the truth), their combined ERA/MME algorithm demonstrated significant improvements in the identification of the structure's natural frequencies as well as model order determination. However, they did not attempt to derive any results for improving upon the identification of the physical mode shapes of the structure. Damping was also excluded from their simulated structure.

In this paper, we develop an algorithm (via noise reduction in the measurements) that is less sensitive to measurement noise and can identify mode shapes accurately. Also, the proposed algorithm demonstrates the ability to identify mode shapes of structures including significant damping. The combined results reveal that mode shape identification is much more dependent on measurement noise than identification of natural frequencies, yet may still be significantly enhanced by combining the ERA and the MME procedures.

Eigensystem Realization Algorithm

The basic development of the state-space realization concept is attributed to Ho and Kalman[10], who introduced the principle of minimum order realization. The Eigensystem Realization Algorithm (ERA) utilizes singular value decomposition to develop a method of minimum order realization. The ERA algorithm has been successfully applied to realization/identification of several structures from experimental data (e.g., Pappa and Juang[6]). We now give a summary of the algorithm.

Consider the discrete-time linear time-invariant dynamic equation

$$x(k+1) = Ax(k) + Bu(k) \tag{1}$$

$$y(k) = Cx(k) \tag{2}$$

where x is the $n \times 1$ state vector, u is the $p \times 1$ input vector, y is the $q \times 1$ output vector; and A, B, and C are $n \times n$, $n \times p$, and $q \times n$ constant matrices, respectively. Two special solutions for Eqs. (1)-(2) are given by Markov parameters as the impulse response,

$$Y(k) = CA^{k-1}B \tag{3}$$

and the initial state response,

$$Y(k) = CA^{k}[x_1(0)\ x_2(0) \ldots x_i(0) \ldots x_p(0)] \tag{4}$$

where $x_i(0)$ represents the i^{th} set of initial conditions. The ERA begins by forming the $r \times s$ block matrix

$$H(k-1) = \begin{pmatrix} Y(k) & Y(k+m_1) & \ldots & Y(k+m_{s-1}) \\ Y(k+l_1) & Y(k+l_1+m_1) & \ldots & Y(k+l_1+m_{s-1}) \\ \vdots & \vdots & \ddots & \vdots \\ Y(k+l_{r-1}) & Y(k+l_{r-1}+m_1) & \ldots & Y(k+l_{r-1}+m_{s-1}) \end{pmatrix} \tag{5}$$

where r and s are arbitrary integers satisfying the inequalities $rq \geq n$, $sp \geq n$, and l_i $(i = 1, 2, ..., r-1)$ and m_j $(j = 1, 2, ..., s-1)$ are arbitrary integers. For the initial state response measurements, $H(k-1)$ is replaced by $H(k)$. From Eqs. (3)-(5) it can be shown that

$$H(k) = V_r A^k W_s \tag{6}$$

where

$$V_r = \begin{pmatrix} C \\ CA^{l_1} \\ \vdots \\ CA^{l_{r-1}} \end{pmatrix}$$

$$W_s = \begin{pmatrix} B \\ A^{m_1}B \\ \vdots \\ A^{m_{s-1}}B \end{pmatrix}^T$$

V_r and W_s are generalized observability and controllability matrices. The ERA is derived by using singular value decomposition for $H(0)$, defined by

$$H(0) = PDQ^T \tag{7}$$

where P and Q are $rq \times n$ and $sp \times n$ isometric matrices, respectively, and D is a diagonal matrix whose diagonal elements are the positive singular values. The rank n of $H(0)$ is determined by testing the singular values for zero, i.e., by choosing the cutoff magnitude below which the singular values are assumed to represent noise and not modes. The reduced-order realization of dimension n can be constructed by forming

$$A^k = D_n^{-\frac{1}{2}} P_n^T H(k) Q_n D_n^{-\frac{1}{2}} \tag{8}$$

$$B = D_n^{\frac{1}{2}} Q_n^T E_p \tag{9}$$

$$C = E_q^T P_n D_n^{\frac{1}{2}} \tag{10}$$

where P_n and Q_n are formed from the first n columns of P and Q, D_n is an $n \times n$ left upper block matrix, E_p^T is $[I_m, 0]$, and E_q^T is $[I_q, 0]$, where I_p and I_q are identity matrices of order p and q, respectively, and 0 is the zero matrix of appropriate dimensions.

Finally, from the eigensolution of the realized state space matrix A^k, the modal damping ratios and damped natural frequencies are calculated from the real and imaginary parts of the eigenvalues, after transformation from the z to s plane using the relationship

$$s = [ln(z) \pm i2k\pi]/(\Delta\tau) \; ; \qquad i = \sqrt{-1}$$

where

$$z = eigenvalues \; of \; A^k$$

The mode shapes are then calculated using the matrix

$$E_q^T P_n D_n^{\frac{1}{2}} \Psi$$

where

$$\Psi = \textit{eigenvector matrix of } A^k$$

Minimum Model Error Estimation

The idea of filtering noise from measurement data is certainly not unique. Various versions of Kalman filters and other similar algorithms have been extensively studied and implemented (e.g., Gelb[11]; Lewis[12]). A major problem with utilizing traditional filter algorithms is that they require good accuracy in the assumed model for the measured signal. In the case of structural realization/identification, the object of the work is to obtain this model. Therefore, while it is possible that judicious use of a filter-smoother algorithm may benefit the ERA, we have not pursued this approach because of the theoretical modeling difficulties just mentioned.

Recently, a new approach for performing optimal state estimation in the presence of significant model error has been developed by Mook and Junkins[13]. The new technique, called Minimum Model Error (MME) estimation, does not assume that the model error is a white noise of known covariance as do the filters. Instead, the model error is assumed to be an unknown quantity and is estimated as part of the solution. The theoretical advantages of this assumption are obvious for the present problem, since the model is unknown *apriori*. In several previous studies, the MME has been shown to produce state estimates of high accuracy for problems involving both significant model error and significant measurement error (Mook and Lin[14]; Mook[15]; Junkins and Mook[16]). A brief derivation of the Minimum Model Error estimation technique follows.

Given a system whose state vector dynamics is modeled by the (linear or nonlinear) system of equations,

$$\dot{\underline{x}} = \underline{f}[\underline{x}(t), \underline{u}(t), t] \tag{11}$$

where

$\underline{x} \equiv n \times 1$ *state vector*

$\underline{f} \equiv n \times 1$ *vector of model equations*

$\underline{u} \equiv p \times 1$ *vector of forcing terms,*

and given a set of discrete measurements modeled by the (linear or nonlinear) system of equations,

$$\tilde{\underline{y}}(t_j) = \underline{g}_j[\underline{x}(t_j), t_j] + \underline{v}_j \ , \ j = 1, ..., m \tag{12}$$

where

$$\underline{\tilde{y}}(t_j) \equiv r \times 1 \textit{ measurement set at } t_j$$
$$\underline{g} \equiv r \times 1 \textit{ measurement model equations}$$
$$m \equiv \textit{total number of measurement sets}$$
$$\underline{v}_j \equiv r \times 1 \textit{ measurement error vector}$$

where, v_j represents a zero-mean, gaussian random sequence of known covariance R_j, determine the optimal estimate for $\underline{x}(t)$ (denoted by $\underline{\hat{x}}(t)$), during some specified time interval $t_0 \leq t \leq t_f$.

In the MME, the optimal state trajectory estimate is determined on the basis of the assumption that the measurement-minus-estimate error covariance matrix must match the measurement-minus-truth error covariance matrix. This condition is referred to as the "covariance constraint". The covariance constraint is defined mathematically by requiring the following approximation to be satisfied:

$$\left\{[\underline{\tilde{y}}(t_j) - \underline{g}(\underline{\hat{x}}(t_j), t_j)][\underline{\tilde{y}}(t_j) - \underline{g}(\underline{\hat{x}}(t_j), t_j)]^T\right\} \approx R_j \tag{13}$$

Thus, the *estimated measurements* $\underline{g}(\underline{\hat{x}}(t_j), t_j)$ are required to fit the *actual measurements* $\underline{\tilde{y}}(t_j)$ with approximately the same error covariance as the actual measurements fit the truth. Otherwise, the estimate cannot be correct.

The estimated measurement set at time t_j is based on the current state estimate, $\underline{\hat{x}}(t_j)$. The between-measurement state estimate is based on integration of the system dynamic model. Thus, if the system dynamic model contains errors, the integration does not yield the correct state estimate, and the residuals between the estimated and the actual measurements are too large. However, due to the noise in the measurements, it is not appropriate to force the model to predict the measurements exactly. Instead, the measurement-minus-estimate residuals should have the same covariance as the measurement noise. This condition is enforced by the covariance constraint.

When the covariance constraint has been satisfied, the state estimate is considered to have been optimized. If errors are present in the state dynamic equations, satisfaction of the covariance constraint generally requires that these errors be corrected when the model is integrated between measurements. The MME method may be used to produce these model error corrections.

Model error is represented by adding a *to-be-determined* unmodeled disturbance vector $\underline{d}(t)$ to the right-hand sides of the original state model equations, Eq. (11), to produce the modified state governing equations,

$$\dot{\underline{x}} = \underline{f}[\underline{x}(t), \underline{u}(t), t] + \underline{d}(t) \tag{14}$$

Next, the following cost functional is minimized with respect to $\underline{d}(t)$:

$$J = \sum_{j=1}^{m} \left\{[\underline{\tilde{y}}(t_j) - \underline{g}(\underline{\hat{x}}(t_j), t_j)]^T R_j^{-1} [\underline{\tilde{y}}(t_j) - \underline{g}(\underline{\hat{x}}(t_j), t_j)]\right\}$$

$$+ \int_{t_0}^{t_f} \underline{d}(\tau)^T W \underline{d}(\tau) d\tau \tag{15}$$

where

$$W \equiv k \times k \text{ weight matrix to be determined}$$

The functional J in Eq. (15) is the sum of two penalty terms. The first is a weighted sum of discrete terms which penalize the deviation of the predicted measurements (based upon the estimated states) from the actual measurements. Minimization of this summation term tends to drive the state estimates toward values which, when substituted into the measurement model, predict the actual measurements. The weighting R_j^{-1} on each of these penalty terms is the inverse of the associated measurement error covariance; thus, accurate measurements (small R_j) are weighted more heavily than inaccurate measurements (large R_j). The second term in J is an integral term which reflects the assumption that the amount of unmodeled effect to be added should be minimized. However, the unmodeled effect must be sufficient to cause the estimate to satisfy the covariance constraint. The proper balance between the two competing effects depends on the choice of W. The weight matrix, W, is determined such that the covariance constraint is satisfied.

An algorithm for the minimization of J in Eq. (15) follows directly from a modification of the so-called Pontryagin's necessary conditions. For a given W, the minimization of J in Eq. (15) with respect to $\underline{d}(t)$ leads to the TPBVP summarized as:

$$\dot{\underline{x}} = \underline{f}[\underline{x}(t), \underline{u}(t), t] + \underline{d}(t) \tag{14}$$

$$\dot{\underline{\lambda}} = -\left(\frac{\partial \underline{f}}{\partial \underline{x}}\right)^T \underline{\lambda} \tag{16}$$

$$\underline{d} = -\frac{1}{2} W^{-1} \left[\frac{\partial \underline{f}}{\partial \underline{u}}\right]^T \underline{\lambda} \tag{17}$$

$$\underline{x}(t_0) = specified, \quad or \ \underline{\lambda}(t_0^-) = \underline{0} \tag{18}$$

$$\underline{\lambda}(t_j^+) = \underline{\lambda}(t_j^-) + 2H_j^T R_j^{-1} [\underline{\tilde{y}}(t_j) - \underline{g}(\underline{\hat{x}}(t_j), t_j)] \tag{19}$$

$$\underline{x}(t_f) = specified, \quad or \ \underline{\lambda}(t_f^+) = \underline{0} \tag{20}$$

where

$$H \equiv \left.\frac{\partial \underline{g}}{\partial \underline{x}}\right|_{\underline{\hat{x}}(t_j), t_j}$$

If the assumed model in the MME algorithm is linear, then a multiple shooting technique may be used to solve the two-point boundary value problem described by Eqs. (14)-(20). This technique converts the TPBVP into a set of linear algebraic equations which may be solved using any linear equation solver (Lew and Mook[17]). In the present case, the model produced by the ERA and used for input to the MME is always linear, so the MME solution is obtained from linear algebraic equations.

Realized vs. Physical Mode Shapes

Before considering some examples, it is important to become familiar with the relationships describing the physical system's mode shapes. To achieve this, a derivation devoted to the connection between the realized and physical system's mode shapes is provided.

We begin the derivation with the familiar boundary-value problem describing the free vibration of a beam. The boundary-value problem can be reduced to the differential equation

$$\frac{d^2}{dx^2}\left[EA(x)\frac{d^2\Phi(x)}{dx^2}\right] = \omega^2 m(x)\Phi(x), \qquad 0 < x < L$$

and the boundary conditions

$$y(0,t) = y(L,t) = 0$$

where $EA(x)$ is the flexural rigidity, $m(x)$ is the mass per unit length at any point x, $\Phi(x)$ is the eigenfunction related to the mode shapes, and ω is the natural frequency of each corresponding mode shape. Based on the separation of variables, the exact solution can be expressed in the following form:

$$y(x,t) = \sum_{i=1}^{\infty} \phi_i(x)\eta_i(t)$$

For this solution, $\phi_i(x)$ represents the individual mode shapes of the structure depending on the spatial variable x alone, and $\eta_i(t)$ indicates the type of motion the structure exhibits.

Although the free vibration problem for a continuous beam is different from the discretized problem, the general approach to their solutions is the same. Therefore, discretizing the continuous beam, a new system can be defined as having mass, stiffness, and damping matrices M, K, and C respectively and the governing equation

$$M\ddot{x}(t) + C\dot{x}(t) + Kx = 0 \tag{21}$$

This discrete system representation can be transformed into its state space form given below:

$$\begin{pmatrix} \underline{\dot{x}}(t) \\ \cdots \\ \underline{\ddot{x}}(t) \end{pmatrix} = \begin{pmatrix} 0 & \vdots & I \\ \cdots & \cdots & \cdots \\ M^{-1}K & \vdots & M^{-1}C \end{pmatrix} \begin{pmatrix} \underline{x}(t) \\ \cdots \\ \underline{\dot{x}}(t) \end{pmatrix} \tag{22}$$

where,

$$A = \begin{pmatrix} 0 & \vdots & I \\ \cdots & \cdots & \cdots \\ M^{-1}K & \vdots & M^{-1}C \end{pmatrix}$$

Rewriting equation (22) into its familiar form, we obtain

$$\dot{\underline{x}}(t) = A\underline{x}(t)$$

The state space A matrix can be represented in its Jordan canonical form

$$A = P\Lambda P^{-1}$$

where P is the eigenvector matrix and Λ is the diagonal eigenvalue matrix. Therefore, similar to the continuous time problem, the solution to the discretized problem for one specific time takes the following form:

$$\underline{x}(t_i) = P \begin{pmatrix} e^{\lambda_1 t_i + j\Theta_1} \\ e^{\lambda_2 t_i + j\Theta_2} \\ \vdots \\ e^{\lambda_{2n} t_i + j\Theta_{2n}} \end{pmatrix} \tag{23}$$

Now, we extend this solution to include a succession of discrete time values.

$$X = \left(\underline{x}(t_1) \vdots \underline{x}(t_2) \vdots \ \ldots \ \vdots \underline{x}(t_m) \right) = PE, \qquad m \geq 2n$$

where,

$$E = \begin{pmatrix} e^{\lambda_1 t_1 + j\Theta_1} & e^{\lambda_1 t_2 + j\Theta_1} & \ldots & e^{\lambda_1 t_m + j\Theta_1} \\ e^{\lambda_2 t_1 + j\Theta_2} & e^{\lambda_2 t_2 + j\Theta_2} & \ldots & e^{\lambda_2 t_m + j\Theta_2} \\ \vdots & \vdots & \ddots & \vdots \\ e^{\lambda_{2n} t_1 + j\Theta_{2n}} & e^{\lambda_{2n} t_2 + j\Theta_{2n}} & \ldots & e^{\lambda_{2n} t_m + j\Theta_{2n}} \end{pmatrix}$$

The relationship PE becomes the definition of the generalized Hankel matrix and its first derivative is defined as the shifted Hankel matrix. The generalized Hankel matrix is denoted by $H(0)$ and its shifted version is denoted $H(1)$:

$$X = PE = H(0) \tag{24}$$

$$\dot{X} = P\Lambda E = H(1) \tag{25}$$

The next step is to perform the singular value decomposition on the Hankel matrix

$$X = H(0) = U\Sigma V^T$$

or

$$X = H(0) = U\Sigma^{\frac{1}{2}}\Sigma^{\frac{1}{2}}V^T \tag{26}$$

where U and V are isometric matrices and Σ is the diagonal matrix of singular values. The realization that is defined by the Eigensystem Realization Algorithm takes on the following form:

$$\bar{A} = (U\Sigma^{\frac{1}{2}})^{-1}\ H(1)\ (\Sigma^{\frac{1}{2}}V^T)^{-1} \tag{27}$$

or after substituting $H(1) = P\Sigma E$,

$$\bar{A} = \Sigma^{-\frac{1}{2}} U^T \; P\Sigma E \; V\Sigma^{-\frac{1}{2}} \tag{28}$$

Now by setting $U\Sigma^{\frac{1}{2}} = PS$, where S is some unknown matrix that is responsible for this equation being satisfied, we get the following sequence of steps leading to the new definition of $\bar{A}$:

$$H(0) = U\Sigma V^T = U\Sigma^{\frac{1}{2}}\Sigma^{\frac{1}{2}}V^T \tag{29}$$

after substitution of $U\Sigma^{\frac{1}{2}} = PS$, and recalling that $H(0) = PE$ the following relationship holds:

$$PE = PS\Sigma^{\frac{1}{2}}V^T \tag{30}$$

Rearranging to solve for $S^{-1}E$ we obtain

$$S^{-1}E = \Sigma^{\frac{1}{2}}V^T \tag{31}$$

After substitution of Equation (31) and $U\Sigma^{\frac{1}{2}} = PS$ into the Equation (28) we obtain

$$\bar{A} = (PS)^{-1} \; P\Lambda E \; (S^{-1}E)^{-1} \tag{32}$$

Taking the inverses,

$$\bar{A} = S^{-1}P^{-1} \; P\Lambda E \; E^{-1}S \tag{33}$$

and this reduces to the continuous time realization

$$\bar{A} = S^{-1}\Lambda S \tag{34}$$

It now becomes apparent by observing equations (22) and (34) that there is in fact a difference between the realized and physical system's eigenvector matrices. The physical system's eigenvector matrix is P, while the realized system's eigenvector matrix is S^{-1}. However, it is worth noting that the eigenvalues of both systems are identical. Therefore, if we wish to calculate the physical system's eigenvectors, we simply employ the relationship

$$P = U\Sigma^{\frac{1}{2}}S^{-1} \tag{35}$$

where S^{-1} is the realized system's eigenvector matrix.

Enhanced Mode Shape Identification Algorithm

The enhanced (i.e. higher accuracy in the presence of noise) mode shape identification algorithm for robust system realization/identification can be summarized in the following steps.

1. Apply the ERA procedure to the measurements in the usual manner to produce a minimum-order realization model with mode shapes.

2. Input the realized model and the measurements into the MME algorithm to produce optimal state estimates.

3. Sample the MME produced state estimates at discrete-time intervals to create simulated measurements of higher accuracy than the original measurements.

4. Apply ERA to the simulated measurements in order to realize/identify the new mode shapes.

5. Examine the newly calculated mode shapes for some convergence criteria, and repeat the procedure if necessary.

Examples

The intent of the following examples is to contrast the mode shape identification abilities of the proposed algorithm verses ERA by itself. Consider the axial vibrations of a cantilever aircraft wing illustrated below in Figure 1.

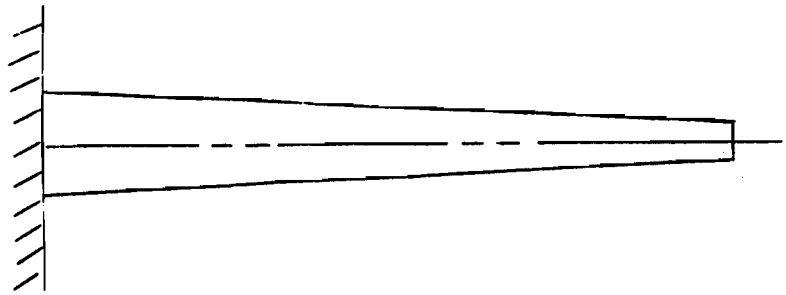

Figure 1 Cantilever Aircraft Wing

Rather than solving the continuous differential eigenvalue problem (Meirovitch[18]), the approach taken here is to discretize the cantilever wing into a four degree-of-freedom system consisting of four masses with idealized springs and dampers between each mass. The governing equations of the discrete system are transformed into the state space form shown below and the proper constants for each mass, spring, and damper substituted.

$$\begin{pmatrix} \dot{\underline{x}}(t) \\ \cdots \\ \ddot{\underline{x}}(t) \end{pmatrix} = \begin{pmatrix} 0 & \vdots & I \\ \cdots & \cdots & \cdots \\ M^{-1}K & \vdots & M^{-1}C \end{pmatrix} \begin{pmatrix} \underline{x}(t) \\ \cdots \\ \dot{\underline{x}}(t) \end{pmatrix}$$

For the first example, $C = 0$ with M and K equal to:

$$M = \begin{pmatrix} 1 & 0 & 0 & 0 \\ 0 & 1 & 0 & 0 \\ 0 & 0 & 1 & 0 \\ 0 & 0 & 0 & 1 \end{pmatrix}; \quad K = \begin{pmatrix} 10 & -5 & 0 & 0 \\ -5 & 10 & -5 & 0 \\ 0 & -5 & 10 & -5 \\ 0 & 0 & -5 & 10 \end{pmatrix}$$

For the second example, M and K stay the same but,

$$C = \begin{pmatrix} 0.3 & 0 & 0 & 0 \\ 0 & 0.3 & 0 & 0 \\ 0 & 0 & 0.3 & 0 \\ 0 & 0 & 0 & 0.3 \end{pmatrix}$$

Utilizing the matrix exponential, the exact time domain solution of each example is calculated. The exact mode shapes, natural frequencies, and damping ratios are then calculated by ERA using the exact time domain solution as input measurements.

For the first example, no damping was included in the system's model (C=0). Assuming only positional measurements are available, the exact solution as given by ERA is indicated in Tables 1.1 and 1.2. The solution consists of the singular values (revealing the number of modes identified), the eigenvalues (indicating each modes natural frequency and damping ratio), and the mode shapes. It should be noted that each mode identified is normally associated with a pair of singular values. However, for simplicity each pair of singular values is averaged together so that the number of nonzero averaged singular values equals the number of modes identified.

With the exact solution known, a gaussian distributed white noise approximately 5-10% the size of the signal amplitude is added to the perfect measurements to investigate the performance of each algorithm. The results of the stand alone Eigensystem Realization Algorithm processing the noisy measurements are displayed in Tables 1.3 and 1.4. Examining the singular values of Table 1.3, one would conclude that only 3 modes were identified, and the remaining nonzero singular values represented noise in the measurements. Directly related to this, a pair of eigenvalues and its corresponding mode shape were completely unidentifiable. Therefore, due to measurement uncertainty the ERA algorithm only identified 3 of the 4 participating modes. Moreover, comparing Table 1.1 with Table 1.3 we see that the identification of the eigenvalues is very poor. Similarly, comparing Table 1.2 with Table 1.4, the mode shape identification is poor.

TABLE 1.1

Exact Solution Of Example # 1

Singular Values	Eigenvalues
17.706	0.000 ± 4.253i
10.192	0.000 ± 3.618i
3.215	0.000 ± 2.629i
0.269	0.000 ± 1.382i
0.000	
0.000	
0.000	
0.000	

TABLE 1.2

Exact Mode Shapes (4 discrete points)

Mode 1	Mode 2	Mode 3	Mode 4
0.3717	-0.6015	0.6015	-0.3717
0.6015	-0.3717	-0.3717	0.6015
0.6015	0.3717	-0.3717	-0.6015
0.3717	0.6015	0.6015	0.3717

TABLE 1.3

Stand Alone ERA Results

Singular Values	Eigenvalues
17.692	-0.07495 ± 4.0421i
10.282	-9.53686 + 62.8312i
3.132	-33.8623 + 0.00000i
0.398	-0.02049 ± 2.6538i
0.306	-0.01701 ± 1.3841i
0.278	
0.256	
0.240	

TABLE 1.4

ERA Identified Mode Shapes (4 discrete points)

Mode 1	Mode 2	Mode 3	Mode 4
0.4012	-0.5945	0.2087	-0.0751
0.5743	-0.3622	0.2532	0.4508
0.5912	0.4039	0.1717	-0.7844
0.3992	0.6069	0.3515	0.6279

Note: The final tabulated results for both algorithms given in Tables 1.3-1.6 are an average of 10 individual results provided by 10 different seeds of a random number generator. This truncated use of a Monte Carlo analysis produced convergence upon the true mode shapes, otherwise not obtained for individual cases. Therefore, in analyzing "real world" problems, taking many different sets of measurements and averaging the results should produce more reliable results.

Tables 1.5 and 1.6 give the results of the Enhanced Mode Shape Identification Algorithm proposed in this paper. For this particular example only two cycles of the procedure summarized above were needed for convergence. Examining the singular values of Table 1.5, one would conclude that 4 modes were identified by the enhanced algorithm and the remaining singular values represented noise. Notice, the mode not identified by the stand alone ERA is accurately recovered by the combined algorithm. Also, the other three mode shapes are more precisely identified. The improved accuracy of the eigenvalues is also apparent. For this example, the true mode shapes and those identified by ERA alone (measurements), and the enhanced algorithm (estimate) are illustrated in Figures 2 through 5.

TABLE 1.5

Enhanced Algorithm Results

Singular Values	Eigenvalues
17.654	-0.04505 ± 4.343i
10.159	-0.19430 ± 3.798i
3.204	-0.02898 ± 2.634i
0.301	-0.01298 ± 1.393i
0.089	
0.080	
0.071	
0.064	

TABLE 1.6

Enhanced Algorithm Mode Shapes

Mode 1	Mode 2	Mode 3	Mode 4
0.3705	-0.5685	0.5645	-0.3223
0.6098	-0.3810	-0.4193	0.6001
0.6005	0.3711	-0.3486	-0.7101
0.3891	0.6395	0.6312	0.4541

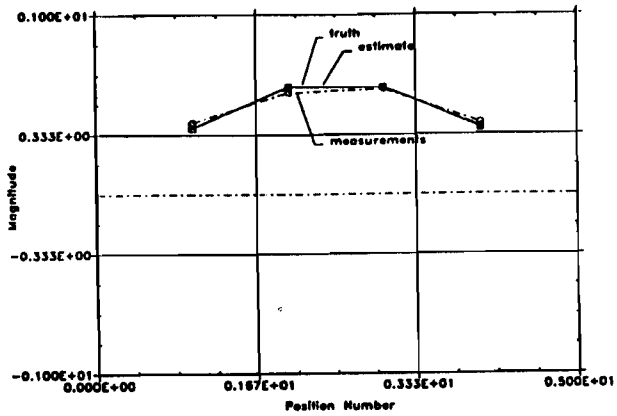

Figure 2 Mode Shape # 1 (no damping)

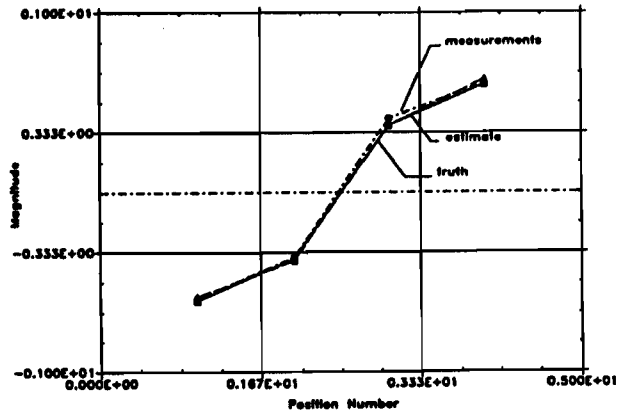

Figure 3 Mode Shape # 2 (no damping)

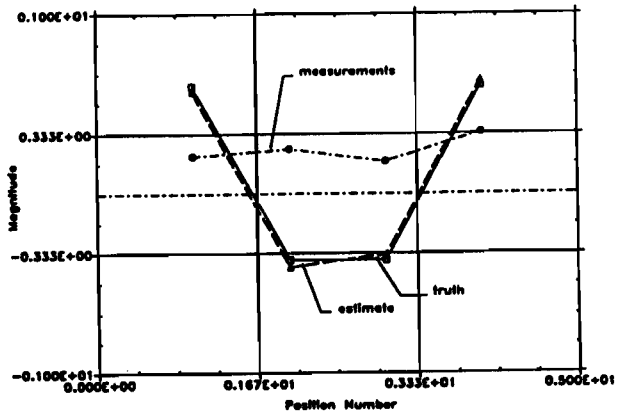

Figure 4 Mode Shape # 3 (no damping)

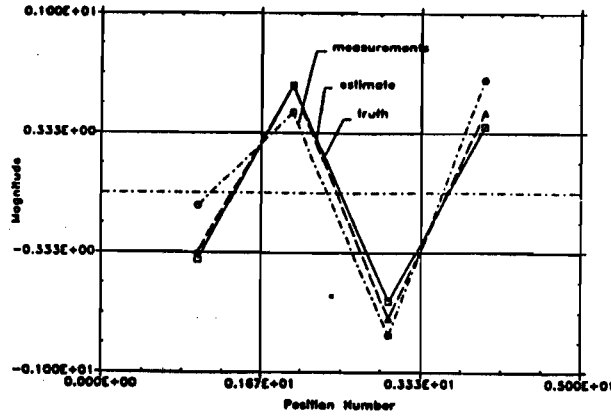

Figure 5 Mode Shape # 4 (no damping)

In the second example, the system's model includes proportional damping exceeding a 15% damping ratio. The results were calculated in the same fashion as the previous example. The results are given in Tables 2.1 through 2.6. Again, by examination of the singular values of Table 2.3, it is obvious that only 3 modes were identified by ERA and the remaining nonzero singular values represented noise in the measurements. Also, the same pair of eigenvalues and its corresponding mode shape were not identified. Therefore, due to the combination of measurement uncertainty and structural damping, the ERA algorithm only identified 3 modes.

TABLE 2.1

Exact Solution Of Example # 2

Singular Values	Eigenvalues
13.298	-0.1500 ± 4.250i
7.023	-0.1500 ± 3.615i
2.374	-0.1500 ± 2.624i
0.197	-0.1500 ± 1.374i
0.000	
0.000	
0.000	
0.000	

TABLE 2.2

Exact Mode Shapes (4 discrete points)

Mode 1	Mode 2	Mode 3	Mode 4
0.3717	-0.6015	0.6015	-0.3717
0.6015	-0.3717	-0.3717	0.6015
0.6015	0.3717	-0.3717	-0.6015
0.3717	0.6015	0.6015	0.3717

TABLE 2.3

Stand Alone ERA Results

Singular Values	Eigenvalues
13.132	-0.4637 ± 4.0391i
6.931	-15.9319 + 0.00000i
2.332	-76.8623 + 62.8318i
0.326	-0.17097 ± 2.6627i
0.289	-0.17551 ± 1.3721i
0.262	
0.250	
0.239	

TABLE 2.4

ERA Identified Mode Shapes (4 discrete points)

Mode 1	Mode 2	Mode 3	Mode 4
0.4048	-0.5982	0.5294	-0.0482
0.5613	-0.3470	0.5839	0.4502
0.5971	0.4052	0.5217	-0.7690
0.4067	0.6154	-0.1205	0.6332

Tables 2.5 and 2.6 show the results of the Enhanced Mode Shape Identification Algorithm for the second example including damping. Similar to the first example, only two cycles of the algorithm's summarized steps were necessary for convergence. The singular values listed in Table 2.5 show that 4 modes were identified by the proposed algorithm as opposed to the 3 modes identified by ERA. The mode not identified by the stand alone ERA was again accurately identified by the combined algorithm. The illustrations of the mode shapes identified by both algorithms are given in Figures 6 through 9. The presence of damping in the structure did effect the mode shape identification, however, an accurate recovery of all four mode shapes was still obtained.

TABLE 2.5
Enhanced Algorithm Results

Singular Values	Eigenvalues
13.219	-0.29915 ± 4.3243i
7.668	-0.28050 ± 3.7947i
2.235	-0.17647 ± 2.6355i
0.232	-0.16090 ± 1.3871i
0.098	
0.090	
0.077	
0.069	

TABLE 2.6
Enhanced Algorithm Mode Shapes

Mode 1	Mode 2	Mode 3	Mode 4
0.3901	-0.6165	0.4645	-0.3165
0.5843	-0.3767	-0.2193	0.6341
0.5943	0.3825	-0.4486	-0.5622
0.3965	0.5983	0.7312	0.4541

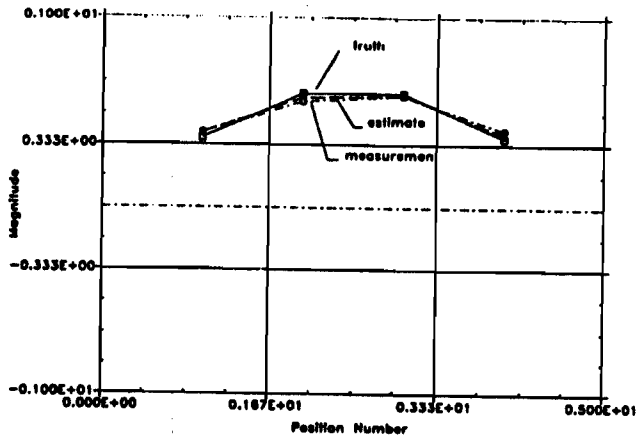

Figure 6 Mode Shape # 1 (with damping)

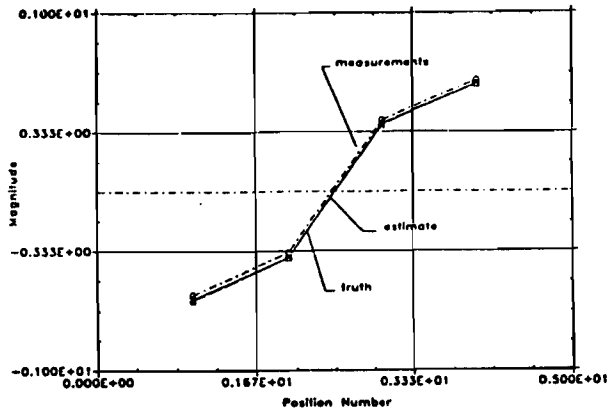

Figure 7 Mode Shape # 2 (with damping)

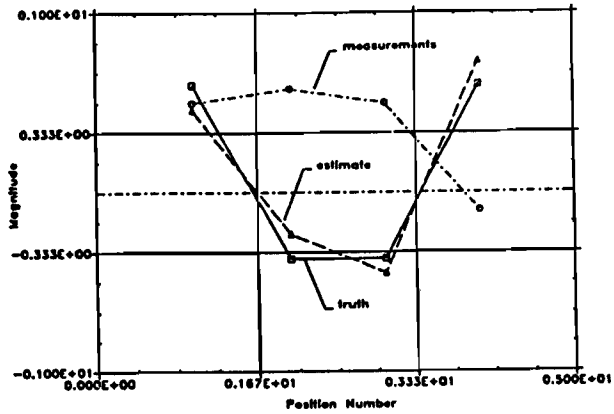

Figure 8 Mode Shape # 3 (with damping)

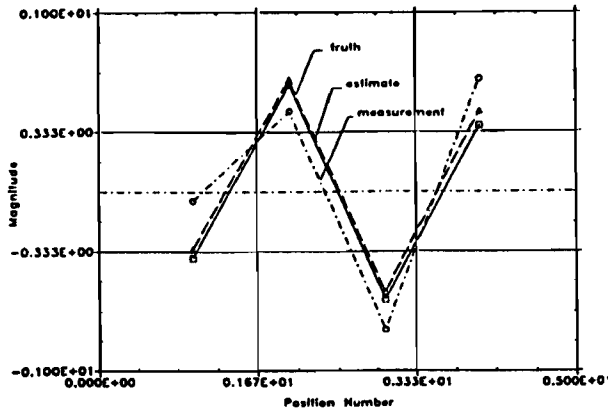

Figure 9 Mode Shape # 4 (with damping)

Complex Mode Identification

The mode shapes identified in the previous two examples are refered to as real or normal modes. Normal modes are identified in hypothetical systems that are most commonly characterized by mathematical models that assume either no damping or proportionally distributed damping of the form

$$[C] = \alpha[M] + \beta[K]$$

The required assumptions for normal mode systems is in many cases very accurate and is therefore commonly used. For example, the off-diagonal damping terms of the [C] matrix (often producing non-proportional damping) are often regaurded as very small and therefore are neglected. In addition, the physical interpretation of normal modes is easily attained. However, for structures involving the use of composite materials or possessing concentrated damping sources the structure can only be accurately modeled using complex modes.

Identification of complex modes is most commonly associated with structures exhibiting significant "non-proportional" damping distributions. In a more general sense, complex modes will be present if the coefficient matrices of a discretized lumped-mass system do not commute as shown below.

$$[C][M]^{-1}[K] \neq [K][M]^{-1}[C]$$

Recall that this is also the condition for a system that cannot be diagonalized. As one would expect, complex mode shapes are difficult to construe in a physical sense. The common desciption of such a phenomenon is demonstrated by drifting nodal locations in an animated mode shape display. In other words, the phase angles associated a particular complex mode are not in phase with each other.

The ERA technique and inturn the robust mode shape identification algorithm introduced in this paper are capable of identifying complex modes. The original ERA derivation was conducted in a normal mode basis. Therefore, the real modes have zero degree phase angles as compared to a complex mode formulation where the real modes possess phase angles of $\pm 45°$ or $\pm 135°$. In either case, a real mode can easily be determined if the phase angles are equal or 180° out of phase. In many circumstances, the ability to identify complex modes is essential to the development of mathematical models that can accurately describe the motions of particular structures.

To demonstrate the ability of complex mode identification, an example is provided that involves this type of computation. As previously stated, complex modes are frequently produced by concentrated damping in isolated locations of a structure. To simulate this type of damping while continuing to utilize the previous example's mass and stiffness matrices the following damping matrix was employed.

$$C = \begin{pmatrix} 2.0 & 0 & 0 & 0 \\ 0 & 0 & 0 & 0 \\ 0 & 0 & 0 & 0 \\ 0 & 0 & 0 & 0 \end{pmatrix}$$

For this example, the same procedure was utilized as the previous two examples with respect to the singular values and eigenvalues. However, the complex modes can not be illustrated as in the normal mode case. Instead, the complex mode shapes are tabulated with respect to the magnitude and phase angles of each complex number contained in the respective mode shapes. Note; if the four complex numbers representing each mode shape were plotted in the complex plane and they formed a straight line, then the mode shape is a normal mode. Table 3.1 represents the true eigenvalues and calculated singular values of the simulated four degree-of-freedom structure. One can plainly see the four distinct modes. Table 3.2 contrasts the ERA algorithm's results with those of the robust mode shape identification algorithm. Examining the singular values of each algorithm one would determine that only 3 modes were identified by the ERA while all 4 modes were recognized by the enhanced algorithm. These results are in agreement with the previous two examples.

TABLE 3.1

Exact Solution Of Complex Mode Example

Singular Values	Eigenvalues
12.852	-0.06446 ± 4.1785i
6.401	-0.34364 ± 3.3992i
3.721	-0.45722 ± 2.7047i
0.282	-0.13467 ± 1.4209i
0.000	
0.000	
0.000	
0.000	

TABLE 3.2

ERA and Enhanced I.D. Algorithm Comparison

ERA ALONE		ENHANCED ALGORITHM	
Singular Values	Eigenvalues	Singular Values	Eigenvalues
12.362	-0.19156 ± 4.0624i	12.423	-0.06031 ± 4.1672
6.942	-77.4706 + 62.831i	6.925	-0.30825 ± 3.2153
3.360	-11.0999 + 0.0000i	3.410	-0.65604 ± 2.6112
0.324	-0.29788 ± 2.6670i	0.275	-0.13634 ± 1.4209
0.298	-0.15241 ± 1.4044i	0.0834	
0.274		0.0756	
0.266		0.0641	
0.251		0.0556	

The last four tables, Table 3.3 through Table 3.6, are the complex mode shapes of the exact solution, those identified by ERA alone, and the enhanced identification algorithm. The results presented here are even more substantial than the previous two cases. Notice complex modes number 3 and 4, niether of these modes were identified very well by the

ERA algorithm alone. However, all four complex modes were identified accurately by the robust mode shape identification algorithm. These results are observed clearly in the following tables.

TABLE 3.3

Complex Mode # 1

Truth	ERA Alone	Robust Algorithm
0.374 + 19.0°	0.437 + 13.0°	0.387 + 19.4°
0.607 + 1.4°	0.584 + 1.2°	0.589 + 1.5°
0.619 - 4.9°	0.602 - 5.3°	0.619 - 5.3°
0.386 - 7.6°	0.371 - 7.8°	0.391 - 7.4°

TABLE 3.4

Complex Mode # 2

Truth	ERA Alone	Robust Algorithm
0.826 + 13.1°	0.622 + 5.1°	0.864 + 8.7°
0.585 - 42.9°	0.450 - 24.2°	0.497 - 45.0°
0.414 - 150.2°	0.377 - 152.3°	0.423 - 148.6°
0.544 + 169.3°	0.633 + 178.8°	0.431 + 171.4°

TABLE 3.5

Complex Mode # 3

Truth	ERA Alone	Robust Algorithm
0.824 - 36.3°	0.543 + 0.0°	0.805 - 85.0°
0.815 - 151.8°	0.579 + 0.0°	0.839 - 163.6°
0.383 + 136.5°	0.511 - 0.0°	0.364 + 101.5°
0.698 + 14.9°	0.324 - 180.0°	0.791 + 10.5°

TABLE 3.6

Complex Mode # 4

Truth	ERA Alone	Robust Algorithm
0.268 - 52.0°	0.114 + 171.1°	0.183 - 79.1°
0.584 + 173.9°	0.328 + 177.2°	0.523 + 169.7°
0.696 + 4.6°	0.713 + 0.70°	0.705 + 4.1°
0.465 - 171.3°	0.609 - 179.0°	0.515 - 174.2°

Summary and Conclusions

The successful results of the proposed algorithm convey significant improvements when identifying mode shapes in structures with corrupted output measurements. For instance, when the example structures were subjected to a 5-10% noise level, one mode shape was completely unidentifiable using the Eigensystem Realization Algorithm alone (with and without damping). However, when the enhanced mode shape identification algorithm was tested under the same circumstances, all four mode shapes could be identified accurately (with and without damping). These results are consistent with the singular values calculated from the realized state matrix. The cutoff point (indicating the number of modes identified) for the singular values of Tables 1.3 and 2.3 (ERA) was clearly 3, while the cutoff for Tables 1.5 and 2.5 (enhanced algorithm) was clearly 4.

Examining the the complex mode example, we found significant improvements when identifying the third and forth modes. These robust results can inpart be contributed to the fact that no assumptions were made reguarding the model error in the estimation procedure. This infact is especially suited for identifying modes that are not excited very much in the testing procedure. The advantages of such a technique become obvious to the modal testing community.

Also, for noise levels less than 3% of the signal amplitude both algorithms could identify all four mode shapes, while for noise levels exceeding 15% different combinations of identified modes were observed. However, in all cases the Enhanced Mode Shape Identification Algorithm gave improved results. These results confirm the robust nature of the enhanced mode shape identification algorithm and demonstrate structural realization/identification of mode shapes in the presence of high measurement noise.

Acknowledgements

This work was partially supported by the Air Force Office of Scientific Research (Dr. Anthony Amos, contract monitor) and NASA Langley Research Center (Dr. Jer-Nan Juang, contract monitor). This support is gratefully acknowledged.

References

1. Hendricks, S.L., et. al., "Identification of Mass, Damping, and Stiffness Matrices for Large Linear Vibratory Systems", **AIAA Journal of Guidence, Control, and Dynamics**, Vol. 7, No. 2, pp. 244-245, March-April 1984.

2. Ibrahim, S.R., and Mikulcik, E.C., "A Method for the Direct Identification of Vibration Parameters from the Free Response," **Shock and Vibration Bulletin**, No. 47, Pt. 4, pp. 183-198, Sept. 1977.

3. Rajaram, S., and Junkins, J.L.,"Identification of Vibrating Flexible Structures", **AIAA Journal of Guidance, Control, and Dynamics**, Vol. 8, No. 4, pp. 463-470, July-Aug. 1985.

4. Chen, J.C., et.al., "Direct Structural Parameter Identification by Modal Test Results", 24th Structures, Structural Dynamics, and Materials Conference, Pt. 2, 1983.

5. Juang, J.-N., and Pappa, R.S., "An Eigensystem Realization Algorithm (ERA) for Modal Parameter Identification and Model Reduction", **AIAA Journal of Guidance, Control, and Dynamics**, Vol. 8, No. 5, pp. 620-627, Sept.-Oct. 1985.

6. Pappa, R.S., and Juang, J.-N., "Galileo Spacecraft Modal Identification Using an Eigensystem Realization Algorithm", **Journal of the Astronautical Sciences**, Vol. 33, pp. 15-33, Jan.-Mar. 1985.

7. Juang, J.-N., and Pappa, R.S., "Effects of Noise on Modal Parameters Identified by the Eigensystem Realization Algorithm", **AIAA Journal of Guidance, Control, and Dynamics**, Vol. 9, No. 3, pp. 294-303, May-June 1986.

8. Klema, V.C., and Laub, A.J., "The Singular Value Decomposition: Its Computation and Some Applications",**IEEE Transactions on Automatic Control**, Vol. AC-25, No. 2, pp. 164-176, April 1980.

9. Mook, D.J., and Lew, J.S., "A Combined ERA/MME Algorithm for Robust System Realization/Identification", Proceedings of the 29th Structures, Structural Dynamics, and Materials Conference, Williamsburg, Virginia, April 1988.

10. Ho, B.L., and Kalman, R.E., "Effective Construction of Linear State-Varable Models From Input/Output Data", 3^{rd} Annual Allerton Conference on Circuit and System Theory, pp.

449-459, 1965.

11. Gelb, A., editor, **Applied Optimal Estimation**, MIT Press, Cambridge, Massachusetts, 1984.

12. Lewis, F.L., **Optimal Estimation**, Wiley-Interscience Publication, New York, 1986.

13. Mook, D.J., and Junkins, J.L., "Minimum Model Error Estimation for Poorly Modeled Dynamic Systems", **AIAA Journal of Guidance, Control, and Dynamics**, Vol. 11, No. 4, pp. 367-375, May-June. 1988.

14. Mook, D.J., and Lin, J.-C., "Minimum Model Error Estimation of Modal Truncation Errors", Proceedings of the 1987 Spring Meeting of the Society for Experimental Mechanics, Houston, TX, June 1987.

15. Mook, D.J., "Estimation and Identification of Nonlinear Dynamic Systems", Proceedings of the 29^{th} Structures, Structural Dynamics, and Materials Conference, Williamsburg, Virginia, April 1988. Also, to appear, **AIAA Journal**.

16. Junkins, J.L., and Mook, D.J., **Enhanced Spacecraft Attitude Estimation**, Final Report, Contract No. N60921-83-G-9-A165, Naval Surface Weapons Center, Dahlgren, Virginia, 1985.

17. Lew, J.S., and Mook, D.J., "Two-Point boundary Problems Containing Jump Discontinuities", in Review.

18. Meirovitch, L., **Elements of Vibration Analysis**, McGraw-Hill, New York, 1975.